Journal of Colloid and Interface Science 506 (2017) 319–328

Contents lists available at ScienceDirect

Journal of Colloid and Interface Science

journal homepage: www.elsevier.com/locate/jcis

Regular Article

Visual and reversible carbon dioxide sensing enabled by doctor blade coated macroporous photonic crystals

Yi-Han Lin, Shing-Yi Suen, Hongta Yang *

Department of Chemical Engineering, National Chung Hsing University, 145 Xingda Road, Taichung City, 40227, Taiwan

GRAPHICAL ABSTRACT

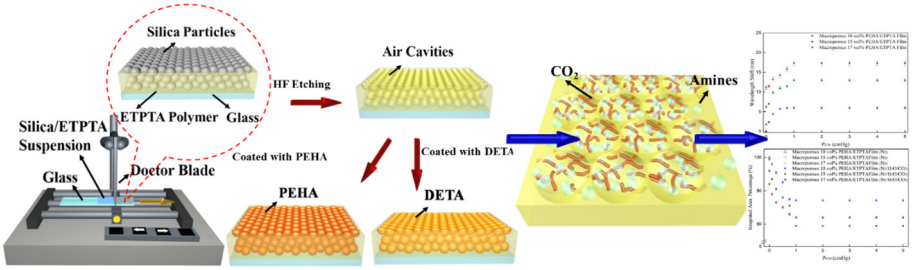

ARTICLE INFO

Article history:
Received 19 May 2017
Revised 7 July 2017
Accepted 8 July 2017
Available online 12 July 2017

Keywords:
Self-assembly
Photonic crystals
Doctor blade coating
Carbon dioxide

ABSTRACT

With significant impacts of carbon dioxide on global climate change, carbon dioxide sensing is of great importance. However, most of the existing sensing technologies are prone to interferences from carbon monoxide, or suffer from the use of sophisticated instruments. This research reports the development of reproducible carbon dioxide sensor using roll-to-roll compatible doctor blade coated three-dimensional macroporous photonic crystals. The pores are functionalized with amine groups to allow the reaction with carbon dioxide in the presence of humidity. The adsorption of carbon dioxide leads to red-shift and amplitude reduction of the optical stop bands, resulting in carbon dioxide detection with visible readout. The dependences of the diffraction wavelength on carbon dioxide partial pressure for various amine-functionalized photonic crystals and different humidities in the environment are systematically investigated. In addition, the reproducibility of carbon dioxide sensing has also been demonstrated in this research.

1. Introduction

Since the Industrial Revolution, started in the mid-1700 s when machinery began to replace human labor, fossil fuels had been used primarily for the manufacture industry. However, the utilization of fossil fuel results in the atmospheric level of carbon dioxide increases by around 40% over the past three decades [1]. The raising amount of carbon dioxide in ecosystems causes increasing awareness of the threat posed by the human-induced enhanced greenhouse effect, leading to global warming, extreme heat waves, rising sea levels, ocean acidification, and irreversible climatic events [2,3]. Environmental consequences of climate change directly affect the physical, social, and psychological health of humans [4]. Besides that, in geological monitoring, a sudden increase of released carbon dioxide levels from springs or volcanoes can be taken as a sign to predict potential disasters [5]. Moreover, it is necessary to monitor carbon dioxide in factories, blackdamp and submarine environments to avoid injury and death by asphyxiation in occupational hygiene [6]. To address the rapidly-growing issues, there is an imperative demand to sense carbon dioxide for environmental monitoring, industrial emission control, and process monitoring applications.

* Corresponding author.
E-mail address: hyang@dragon.nchu.edu.tw (H. Yang).

http://dx.doi.org/10.1016/j.jcis.2017.07.031
0021-9797/

The sensing of carbon dioxide in gaseous phase generally are accomplished by various metal oxide semiconductors, infrared spectroscopy, and electrochemical devices [7–10]. Owing to the feasibility of miniaturization, long life time, and low cost, metal oxide semiconductors based sensors have been extensively exploited for detecting carbon dioxide [11]. Nevertheless, the semiconductor based sensors are operated at high temperature, which seriously restrict their applications [12]. Compared with that, carbon dioxide can be analyzed with a range of infrared spectroscopy at room temperature. However, the technologies suffer from high equipment cost and are prone to interferences from carbon monoxide and humidity [13]. Recently, many other methodologies, most of which are electrochemical determination, gas chromatography-mass spectrometry, and field-effect transistors, have also been widely used in carbon dioxide sensing [14–16]. Unfortunately, most of the existing methods are time-consuming, bulky, susceptible to interference, or require complicated detection processes.

Photonic band gap materials, known as photonic crystals, are periodic dielectric structures with a forbidden gap for electromagnetic waves [17–29]. The Bragg diffraction of light caused by periodic structures in the medium can be shifted by tuning the effective refractive index or the inter-plane distance through solvent swelling, mechanical deformation, and applying external stimuli [20–24]. Owing to the stable structural colors, photonic crystals have attracted a great deal of attention as potential candidates for various chemical sensors [25–27]. The optical chemical sensing exhibits several advantages over other sensing technologies, including portability, non-invasiveness, on-line monitoring capability, short response time, and immunity to electromagnetic interface [28–30]. With easily accessible monodisperse colloids, photonic crystals can be created by a variety of convenient and inexpensive colloidal self-assembly processes [31–36]. However, most of current bottom-up methodologies are only favorable for low volume laboratory scale production, and incompatible with mature fabrication [37]. In addition, the photonic crystal-based carbon dioxide sensing relies on refractive index changes that impeded by the inferior gas adsorption abilities, and thus requires special instruments to analysis [26,38]. Although hydrogel photonic crystal-based carbon dioxide sensors are reported in previous studies, the general limitation of mechanical stability has remained a challenge [39,40].

To address the issues, a scalable and roll-to-roll compatible doctor blade coating technology is developed to fabricate three-dimensional macroporous polymer photonic crystals in this work. The surface of photonic crystals can be functionalized with amine groups to allow carbon dioxide to adsorb and react with amines in the presence of humidity in order to enhance the carbon dioxide adsorption capacity [41–43]. The combination of doctor blade coated macroporous photonic crystals and the adsorption of carbon dioxide to amine groups facilitates amplitude reductions of photonic band gaps, leading to direct detection by readable optical signals. Importantly, the reversible adsorption/desorption of carbon dioxide can be achieved by simply applying heating/cooling cycles in ambient environments. Herein, a rapid and visual sensor with reversibility and high selectivity for the sensing of carbon dioxide can be prepared.

2. Experimental section

2.1. Materials and substrates

The reagents used for the synthesis of silica particles including tetraethyl orthosilicate (TEOS) (98%), ammonium hydroxide (28%), and absolute ethanol (99.5%), were obtained from Sigma-Aldrich. Deionized water (18.2 MΩ cm) was used directly from a Millipore A-10 water purification system. Ethoxylated trimethylolpropane triacrylate monomer (ETPTA, SR 454) and photoinitiator, 2-hydro xy-2-methyl-1-phenyl-1-propanone (Darocur 1173), were acquired from Sartomer and Ciba-Geigy, respectively. Diethylenetriamine (DETA, 98%) and pentaethylenehexamine (PHEA, 98%) used for surface functionalization were provided by ACROS Organics and Sigma-Aldrich, respectively. All chemicals and solvents were of reagent quality and used without further purification. Glass microslides (Corning) were cleaned in a 3:1 mixture of concentrated sulfuric acid with 30% hydrogen peroxide for 30 min, rinsed with deionized water, and dried at room temperature before use.

2.2. Instrumentation

A digital camera (Nikon Coolpix L810) was employed to collect images from specimens. The surface morphologies of the specimens were examined with a JEOL 6335 F field-emission scanning electron microscope and a LEO 1530VP field-emission scanning electron microscope. The specimens were slightly sputter-coated with gold prior to imaging. Fourier transform infrared (FTIR) spectra were acquired using a HORIBA FT-720 FTIR spectrometer. Normal incidence optical reflection spectra were performed by an Ocean Optics HR4000 high-resolution fiber-optic UV–visible-near-IR spectrometer using Ocean Optics DT-MINI-2-B as a light source.

2.3. Preparation of silica colloidal suspensions

The synthesis of monodispersed silica particles with 250 nm in diameter was performed by following the StÖber method (Fig. S1) [44]. In the present work, 50 mL of TEOS was rapidly added to a mixture of 22 mL ammonium hydroxide, 50 mL deionized water, and 640 mL absolute ethanol. The solution was stirred at ambient conditions for 24 h, while TEOS was hydrolyzed to form silica particles. The as-synthesized silica particles were purified by multiple centrifugation/redispersion cycles in absolute ethanol to completely remove unreacted TEOS, ammonium hydroxide, and deionized water, followed by dispersing in UV-curable ETPTA monomer with 1 vol% photoinitiator to make a final silica particle volume fraction of 74 vol% using a vortex mixer (Thermolyne). The silica colloidal suspensions were stored in an open vial in dark for 12 h to allow any residual absolute ethanol to evaporate before using.

2.4. Doctor blade coating

One milliliter of the as-prepared silica colloidal suspension was dispensed on an ETPTA wetting layer coated glass microslide (75 × 25 mm). An immobilized doctor blade (Fisher, 40 mm wide) was applied to spread the suspension uniformly on the substrate, and to offer a one-dimensional shear force to align the silica particles at a controlled coating speed. After coating, the specimen was transferred to a pulsed ultraviolet curing system (X Lite 500, OPAS), and the ETPTA monomer was photo-polymerized to create a silica colloidal crystal/polymer composite by exposure to ultraviolet radiation for 5 s.

2.5. Fabrication of surface functionalized macroporous photonic crystals

The templating silica particles were selectively removed by dropping a 2 vol% aqueous hydrofluoric acid solution on the composite for 1 min, followed by rinsing with absolute ethanol. After repeating for 5 cycles, the specimens were dried in a stream of nitrogen to fabricate macroporous ETPTA photonic crystals. The

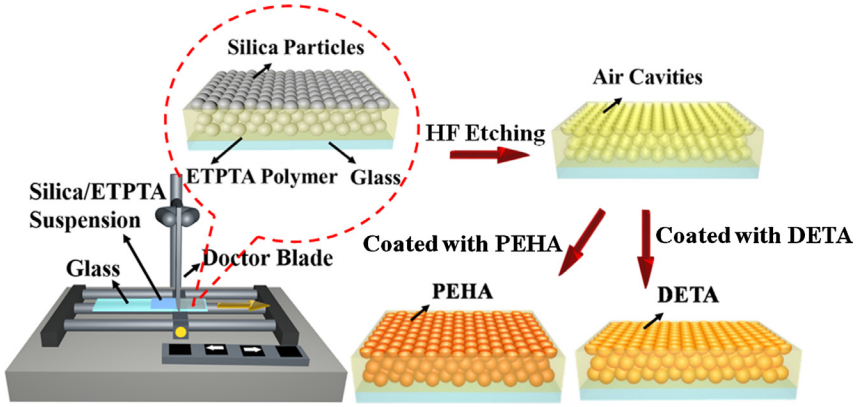

Fig. 1. Schematic illustration of the experimental procedures for fabricating surface functionalized macroporous photonic crystals.

resulting macroporous films were immersed in mixtures of DETA/ethanol or PEHA/ethanol for 2 h under nitrogen atmosphere, and then heated in an oven at 40 °C for 2 h to enable the amine groups of DETA or PEHA to react with the acrylate groups on the film surface [45]. The surface functionalized macroporous films were rinsed with ethanol, following by a spin-coating process to remove the excess chemicals retained on the film.

2.6. Experimental procedures for carbon dioxide detection

The macroporous photonic crystals were placed in a home-made environmental chamber (Fig. S2), which was evacuated and then back-filled with water vapor (2 cm Hg) and carbon dioxide with a specific pressure (evaluated by a Fisher diaphragm vacuum gauge). Dry nitrogen was finally introduced to control the total pressure in the chamber to be 76 cm Hg. A reflection probe connected to a UV–visible-near-IR spectrometer was sealed in the chamber to measure the specular optical reflectance from the photonic crystals at normal incidence, and the spectra were record by Ocean Optics Spectra Suite Spectroscopy Software in the wavelength range from of 400 to 700 nm. In the measurement, the beam spot size was about 3 mm on the specimen surface and the cone angle of collection was less than 5°. Absolute reflectivity was obtained as the ratio of the specimen spectrum and a reference spectrum. Final value of the absolute reflectivity is the average of several measurements collected from different spots on the same specimen.

3. Results and discussion

The schematic illustration of the experimental procedures for fabricating surface functionalized macroporous photonic crystals is displayed in Fig. 1. Three-dimensional silica colloidal crystal/polymer composites are assembled on an ETPTA wetting layer coated glass microslide by a scalable doctor blade coating technodology [46]. The shear-aligned silica colloid crystals embedded in the ETPTA matrix can be removed by etching with an aqueous hydrofluoric acid solution. The resulting macroporous ETPTA films are coated with DETA or PEHA, and heated at 40 °C for 2 h to enable the surface of pores to be functionalized with amine groups.

A photograph of the doctor blade coated silica colloidal crystal/polymer composite consisting of 250 nm silica particles on a glass substrate illuminated with white light is displayed in Fig. 2(a). The specimen exhibits a yellowish color,[1] resulting from Bragg diffraction of incident light from the crystalline lattice as revealed from the top-view scanning electron microscope (SEM) image in Fig. 2 (b). Although point vacancies caused by dust or silica particles with extreme sizes are observed, the long-range hexagonally ordering of silica particles is clearly evident. In addition, the protrusion depth of the top-layer silica particles from composite is smaller than the radius of silica particles, leading to the non-close-packed appearance of silica particles as shown in Fig. 2(c). As a matter of fact, the silica particles are three-dimensionally close-packed and surrounded by an ETPTA matrix (Fig. 2(d)).

The templating close-packed silica colloidal crystals can be removed after a wet etching treatment. As shown in Fig. 3(a), the resulting ETPTA film displays a uniform blue color. The striking color is caused by the Bragg diffraction of visible light from the crystalline lattice of air cavities in the macroporous matrix (Fig. 3 (b)). It is found that the hexagonally ordering of air cavities is well retained during the wet etching procedure. Besides, a magnified top-view SEM image in Fig. 3(c) reveals that the 250 nm air cavities are interconnected through smaller pores that originate from the touching sites of silica particles in the shear-aligned composite. The corresponding contact area between silica particles is not filled with polymer. The cross-sectional SEM image as displayed in Fig. 3 (d) further confirms that the highly ordered air cavities are three-dimensionally face-centered cubic close-packed in the macroporous ETPTA film.

To comprehend the optical properties of the doctor blade coated specimens, the optical reflection spectra measured at normal incidence using a UV–visible-near-IR spectrometer are displayed in Fig. 4. In comparison to featureless ETPTA film (black dotted curve), it is found that the measured reflection peak of the silica colloidal crystal/ETPTA composite consisting of 250 nm silica particles (blue dashed curve) locates at 583 nm. The low refractive index contrast between silica (n_{silica} = 1.42) and ETPTA (n_{ETPTA} = 1.46) leads to a low reflection amplitude. Additionally, the red solid curve displays the measured reflection peak of the corresponding macroporous ETPTA film (red solid curve) locates at 458 nm with high reflection amplitude. This is attributed to the presence of high refractive index contrast between air (n_{air} = 1) and ETPTA in the film. The expected reflection peak positions of the specimens can be theoretically calculated by Bragg's law: [47].

$$\lambda_{peak} = 2n_{eff}d\sin\theta \quad (1)$$

where n_{eff} is the effective refractive index of the medium, d is the inter layer spacing of face-centered cubic close-packed structures, and sinθ equals to 1 at normal incidence. It is noted that the estimated peak positions as presented by the incident arrows are approximately equal to the measured positions, confirming the highly crystalline quality of the self-assembled composite and the

[1] For interpretation of color in Fig. 2a and 4, the reader is referred to the web version of this article.

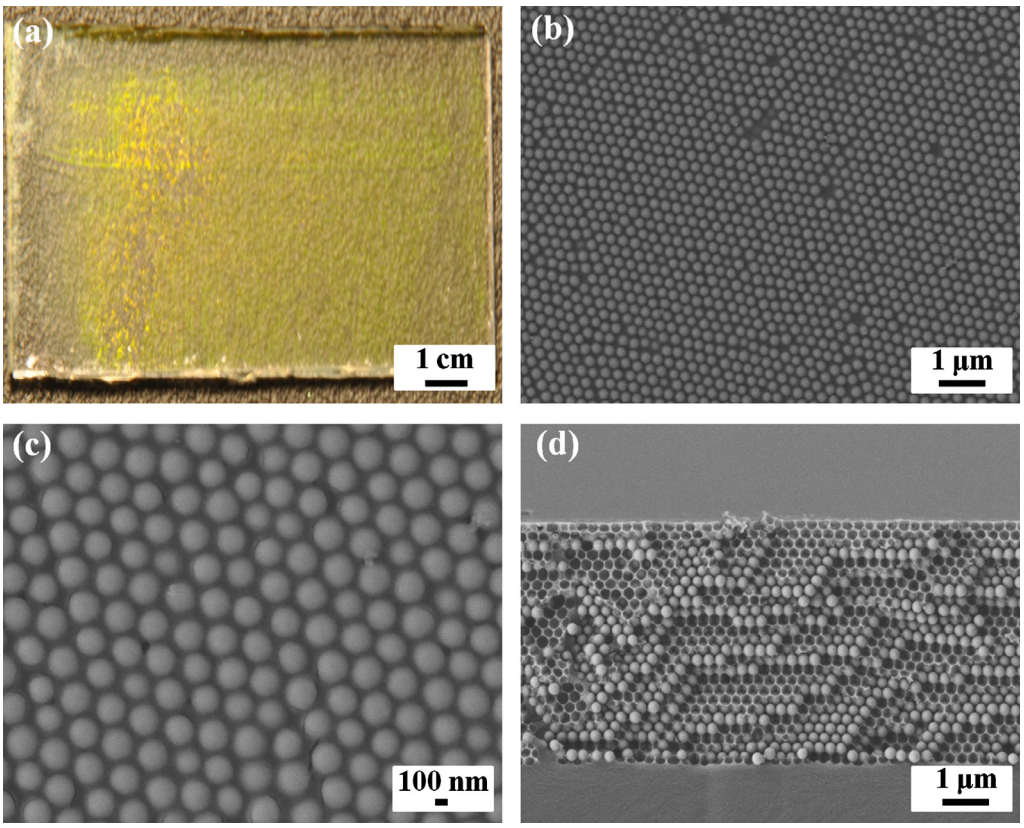

Fig. 2. (a) Photograph of a doctor blade coated silica colloidal crystal/ETPTA composite consisting of 250 nm silica particles. (b) Top-view SEM image of the sample in (a). (c) Magnified SEM image of (b). (d) Cross-sectional SEM image of the sample in (a).

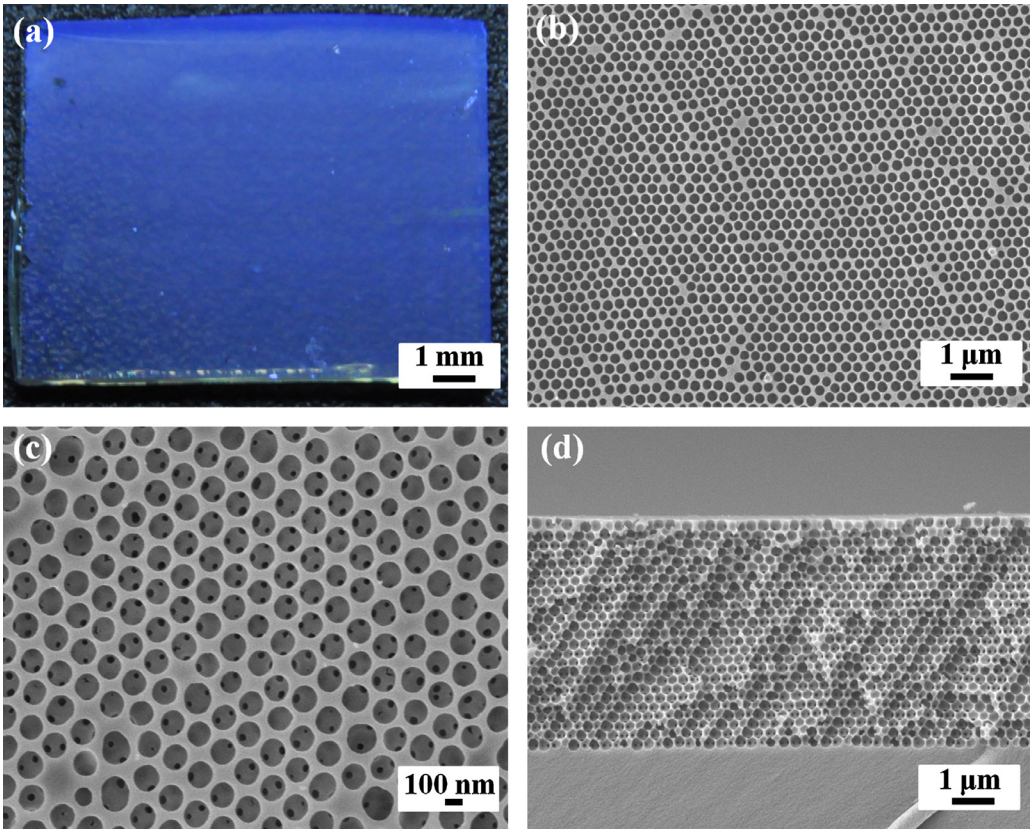

Fig. 3. (a) Photograph of a macroporous ETPTA film templated from 250 nm silica colloidal crystals. (b) Top-view SEM image of the sample in (a). (c) Magnified SEM image of (b). (d) Cross-sectional SEM image of the sample in (a).

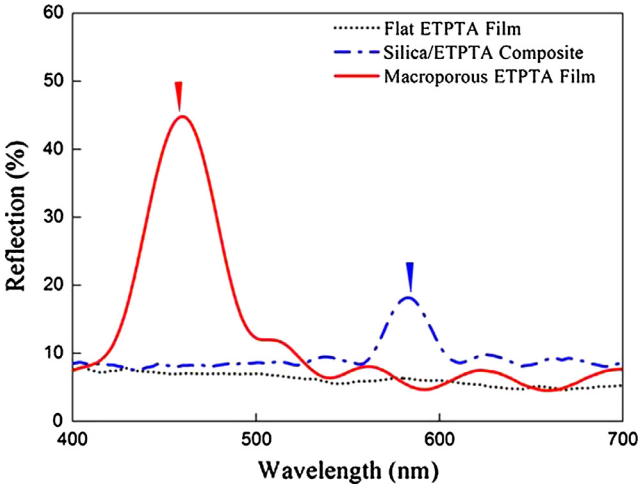

Fig. 4. Normal incidence optical reflection spectra of a flat ETPTA film, a silica colloidal crystal/ETPTA composite consisting of 250 nm silica particles, and a corresponding macroporous ETPTA film. The arrows indicate the expected diffraction peak positions for the composite and the macroporous film, estimated using Bragg's law at normal incidence.

corresponding macroporous film. This further discloses that three-dimensionally close-packed macroporous photonic crystals can be fabricated by the doctor blade coating technology.

The pores of the as-fabricated macroporous film can be functionalized with amine groups, which are highly responsive to carbon dioxide, by using a 10 vol% DETA/ethanol solution to create a macroporous DETA/ETPTA film. The macroporous DETA/ETPTA film as displayed in Fig. S3 (a) exhibits a homogeneous blue color resulted from Bragg diffraction of incident light from three-dimensional ordered air cavities (Fig. S3 (b)–(d)). Similar characteristics can also be found on the macroporous PEHA/ETPTA film, which has been functionalized using a 10 vol% PEHA/ethanol solution (Fig. S4). It is worth mentioning that the air cavities on the films are interconnected even after a surface modification treatment. To explore the effect of surface modification on optical properties, normal incidence optical reflection spectra of the as-prepared macroporous films are compared in Fig. 5(a). It is apparent that the reflection peaks and intensities of the macroporous DETA/ETPTA film and the macroporous PEHA/ETPTA film are quite similar to those of untreated macroporous ETPTA film. The results disclose that the surface modification process does not affect the crystalline quality and optical properties of the macroporous photonic crystals.

In order to identify that the amine groups are functionalized on the macroporous films, Fourier transform infrared (FTIR) spectra of a macroporous ETPTA films, a macroporous DETA/ETPTA film and a macroporous PEHA/ETPTA film are analyzed using a FTIR spectrometer (Fig. 5(b)). For the untreated macroporous ETPTA film, the absorption peaks of carboxylate (C—O), bipyridine (C=C), and carbonyl (C=O) groups are observed at 1167, 1454, and 1735 cm^{-1}, respectively. Additionally, it is noted in passing that bands occurring between 2883 and 2962 cm^{-1} are associated with the symmetric and antisymmetric C—H stretching vibrations of methylene (CH_2) and methyl (CH_3) groups [48]. Comparing with that, it is found that new adsorption peaks centered at 1636 cm^{-1} and 3442 cm^{-1} appear for the macroporous DETA/ETPTA film and the macroporous PEHA/ETPTA film. The bands are assigned to the symmetric and asymmetric amine (N—H) stretching vibrations of DETA or PEHA [49,50]. This further demonstrates the surface of macroporous films are functionalized with amine groups.

To evaluate the carbon dioxide sensing capability of the as-prepared macroporous films, normal incidence optical reflection spectra are collected from the films exposed to carbon dioxide with different partial pressures in the presence of water vapor at 2 cm Hg after 5 min. As noted from Fig. 6(a), water condenses in the air cavities of macroporous ETPTA film, leading to a higher effective refractive index of the diffractive medium and a lower dielectric contrast between the ETPTA matrix and the enclosed materials. This results in the red-shift and the amplitude reduction of the Bragg diffraction peaks. However, the absence of any change in the peak position and amplitude is found when the film is performed under varying carbon dioxide partial pressures. Compared with that, responses are observed as a macroporous DETA/ETPTA film is applied for carbon dioxide sensing (Fig. 6(b)). The responses are mainly caused by the carbon dioxide adsorption on the amine-functionalized ETPTA film (Fig. S5). The amine groups are able to react with the carbon dioxide in the environment to form carbamates, and accompany by the formation of carbamic acids in the presence of water [51,52]. The resulting adsorption leads to the changes of the diffractive medium characteristics [53]. Therefore, the diffraction light of the film red-shifts and the diffraction efficiency of that monotonically decreases as the carbon dioxide partial pressure increases.

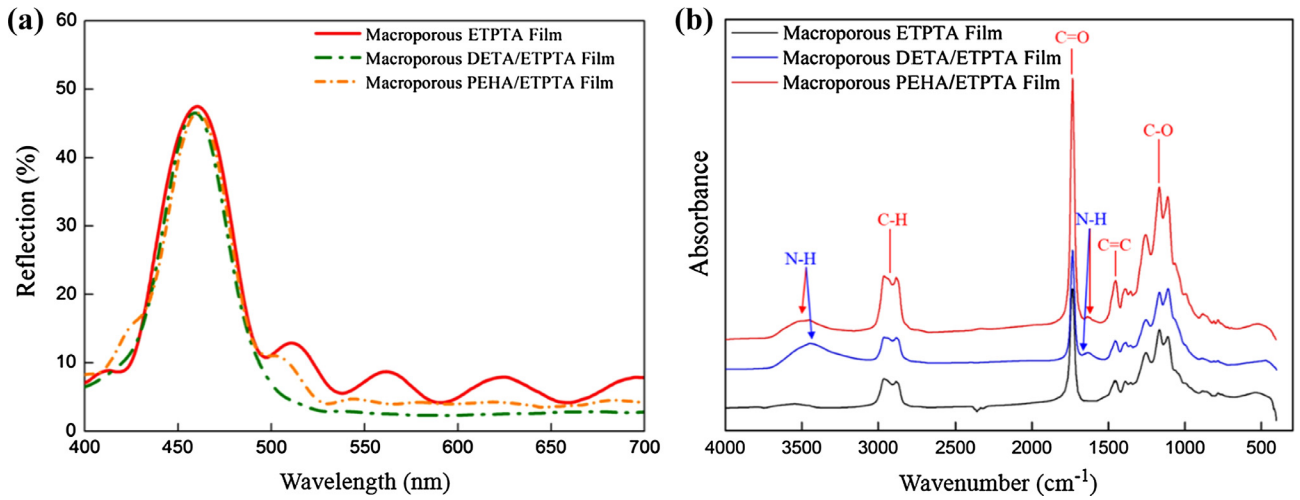

Fig. 5. (a) Normal incidence optical reflection spectra of a macroporous ETPTA film, a macroporous DETA/ETPTA film, and a macroporous PEHA/ETPTA film. The films are all templated from 250 nm silica colloidal crystals. (b) Fourier transform infrared spectra of the macroporous films.

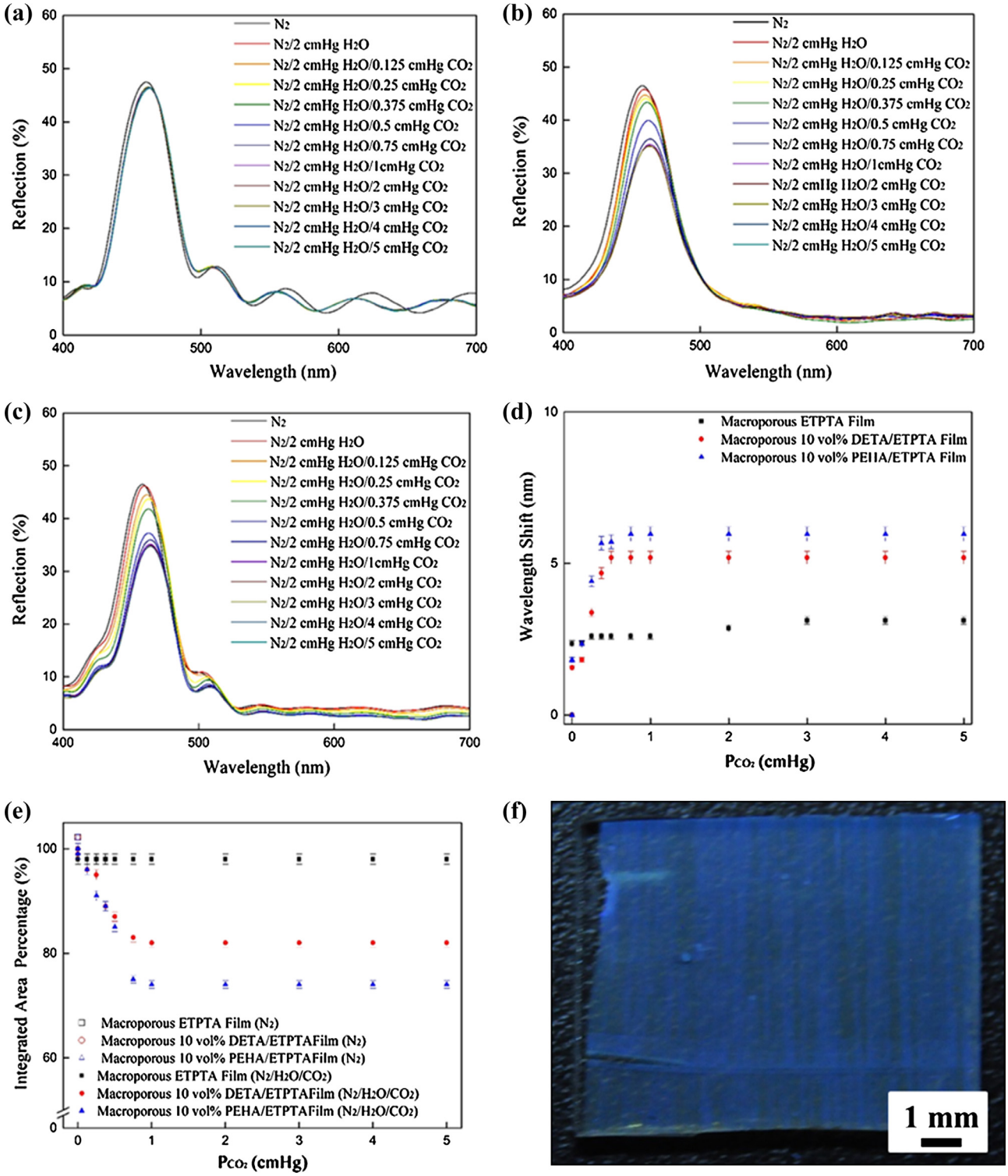

Fig. 6. Normal incidence optical reflection spectra obtained from (a) a macroporous ETPTA film, (b) a macroporous DETA/ETPTA film, and (c) a macroporous PEHA/ETPTA film exposed to carbon dioxide with different partial pressures. The films are all templated from 250 nm silica colloidal crystals. (d) Dependence of the wavelength shift of the Bragg's diffraction peak on carbon dioxide partial pressure. (e) Dependence of the integrated response of the Bragg's diffraction peak on carbon dioxide partial pressure. (f) Photographic image of the macroporous PEHA/ETPTA film exposed to carbon dioxide (1 cm Hg).

In addition, the results in Fig. 6(c) present that the optical response of a macroporous PEHA/ETPTA film is similar with that of a macroporous DETA/ETPTA film in carbon dioxide sensing. It is noteworthy that a macroporous PEHA/ETPTA film exhibits larger red-shift than a macroporous DETA/ETPTA film on exposure to carbon dioxide (Fig. 6(d)). As displayed in Fig. S5 and Fig. S6, the carbon dioxide adsorption mechanisms on a macroporous DETA/ETPTA film and a macroporous PEHA/ETPTA film can be employed to interpret the behavior of carbon dioxide sensing. Due to the increase of amine groups on the macroporous PEHA/ETPTA film, more carbon dioxide can be adsorbed on the film (Fig. S7), actuating a larger red-shift in diffraction. The phenomenon reveals that

the optical response system is controlled by the amount of carbon dioxide relative to the amine groups of the film. Moreover, it is found that the maximum wavelength shift of ~6 nm is achieved as the carbon dioxide partial pressure in the environment reaches 0.5 cm Hg.

To improve the detection sensitivity, a full-peak analysis technology which exploits the amplitude reduction of the Bragg diffraction peaks during carbon dioxide adsorption is developed. Instead of monitoring the small peak shift, the integrated response of Bragg diffraction peak is estimated using the integration tool of the OriginPro 85 software. By taking the response integrated area of the macroporous films exposed to dry nitrogen as 100%, Fig. 6(e) displays that the integrated area percentage of the diffraction peak decreases with the increase of carbon dioxide partial pressure. Importantly, in comparison to the response of a macroporous ETPTA film, a macroporous PEHA/ETPTA film displays remarkable decrease in integrated area percentage. This leads to the macroporous PEHA/ETPTA film presents a lighter blue color as exposed to carbon dioxide (Fig. 6(f)). It is evident that the detection sensitivity is significantly higher than that obtained by conventional peak shift analysis method. Furthermore, the integrated area percentage can reach ~75% when the film is exposed to 0.5 cm Hg carbon dioxide partial pressure, whereas no further decrease is observed under higher carbon dioxide partial pressure. This indicates that excess carbon dioxide cannot be adsorbed on the as-prepared macroporous films, and thus it causes a detection limit.

A higher detection limit can be achieved by increasing the amount of amine groups on the macroporous films. Macroporous ETPTA films templated from 250 nm silica colloidal crystals are immersed in solutions containing 15 vol% PEHA and 17 vol% PEHA, respectively, to fabricate macroporous PEHA/ETPTA films. As presented in Fig. 7(a) and (b), the optical response tendencies of the as-prepared macroporous films on carbon dioxide are similar to those as shown in Fig. 6(b) and (c). The red-shift and amplitude reduction of the diffraction peaks are noticed with the increase of carbon dioxide partial pressure. It is worthy to mention that the higher amount of PEHA on the macroporous 17 vol% PEHA/ETPTA film causes a further increase in the amount of carbon dioxide adsorption, leading to a larger red-shift and amplitude reduction of the optical bands on exposure to carbon dioxide (Fig. 7(c) and (d)). It is also noted that the integrated area percentage of the film reaches ~58% on exposure to 1 cm Hg carbon dioxide partial pressure. The great decrease of luminous intensity can be easily detected by naked eyes (Fig. S8). The results disclose that the sensitivity and detection limit of carbon dioxide sensing are associated with the amount of functionalized amine groups on the film. The amine-functionalized macroporous photonic crystals using 17 vol% PEHA provide a detection range between 0.1 cm Hg and 1 cm Hg, which covers the carbon dioxide partial pressures causing substantial effects on human health risk such as dizziness, headache, nausea, and asphyxiation as carbon dioxide replaces oxygen in the blood when exposed to high levels of carbon dioxide

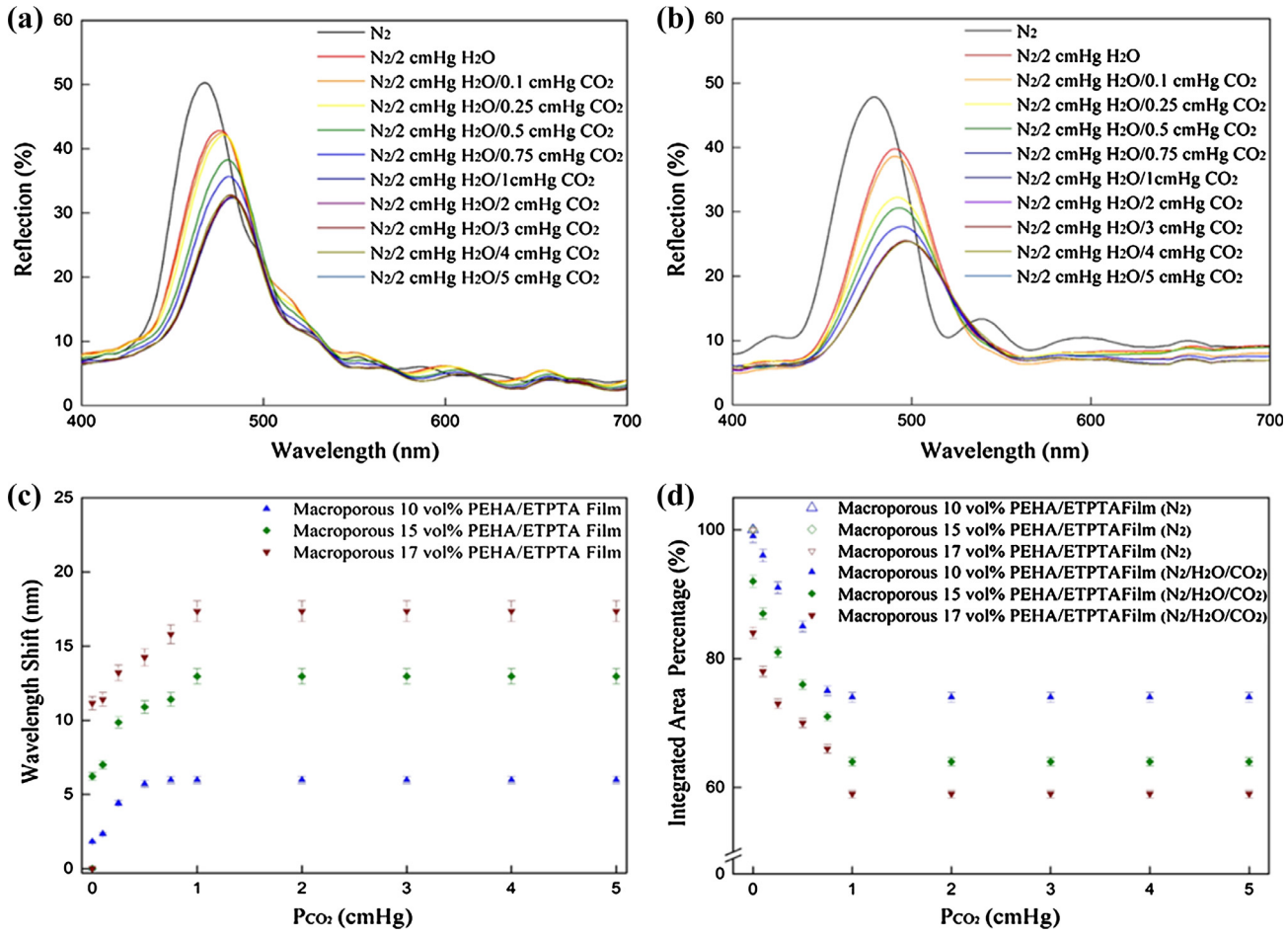

Fig. 7. Normal incidence optical reflection spectra obtained from macroporous PEHA/ETPTA films templated from 250 nm silica colloidal crystals exposed to carbon dioxide with different partial pressures. The macroporous films are coated with solutions containing (a) 15 vol% PEHA and (b) 17 vol% PEHA, respectively, before the measurements. (c) Dependence of the wavelength shift of the Bragg's diffraction peak on carbon dioxide partial pressure. (d) Dependence of the integrated response of the Bragg's diffraction peak on carbon dioxide partial pressure.

for several hours [54]. The detection limit for the as-fabricated sensor using 17 vol% PEHA is 0.1 cm Hg carbon dioxide partial pressure with a ~11 nm red-shift and ~17% amplitude reduction from the blank. Although the directly readable optical signals are suitable for monitoring analytes without using complex instruments, it is not surprising that the minimum quantification limit of the as-prepared sensing materials for carbon dioxide is less sensitive to the detection limits of those traditional methodologies [7–16]. Since the response of photonic crystal-based sensor generally depends on the interaction of an analyte with the sensor surface, increasing the surface area and interspaces for gas adsorption by introducing smaller silica particles can improve the sensing sensitivity through incorporating of a higher surface area to volume ratio [55,56]. Even though further testing is required, it is expected that a lower detection limit can be achieved by increasing the surface area *via* the miniaturization of the photonic crystal sensing materials.

Humidity in the environment is another parameter in evaluating the sensing sensitivity. Therefore, investigations into the effect of humidity on carbon dioxide sensing were conducted in this study. The reflection spectra of macroporous 10 vol% PEHA/ETPTA films templated from 250 nm silica colloidal crystals exposed to carbon dioxide in the presence of water vapor at 1 cm Hg and 0.5 cm Hg are displayed in Fig. 8(a) and (b). It is found that the optical responses are similar with that of the as-fabricated macroporous film exposed to carbon dioxide in the presence of water vapor at 2 cm Hg (Fig. 6(c)). Additionally, when the humidity in the environment is increased, more water vapor condensates in the cavities of the macroporous film, leading to an increase in the amount of carbon dioxide adsorption. This further causes the larger red-shift of the Bragg diffraction peaks and the amplitude reduction of the optical stop bands on exposure to carbon dioxide (Fig. 8(c) and (d)). The results reveal that the sensitivity and the detection range of carbon dioxide sensing can be improved under higher humidity.

It is significant to note that carbamic acids do not react with acrylate groups. Therefore, the carbon dioxide can simply be removed by heating under dry inert environments [57]. At raised temperatures, the equilibrium of carbamic acid formation shifts back to the free amine and carbon dioxide. Therefore, the optical properties of the amine-functionalized macroporous films can be fully recovered and can thus be reused for carbon dioxide sensing. The reproducibility of a macroporous 10 vol% PEHA/ETPTA film templated from 250 nm silica colloidal crystals for carbon dioxide sensing is studied in this research. In the environment of 1 cm Hg carbon dioxide partial pressure, the diffraction peak of the macroporous film is red-shifted from 459 nm to 465 nm, while the integrated area percentage is reduced until it reaches 75%. The film is then heated at 110 °C for 30 min to allow desorption of carbon dioxide and water. The procedures are repeated for several cycles

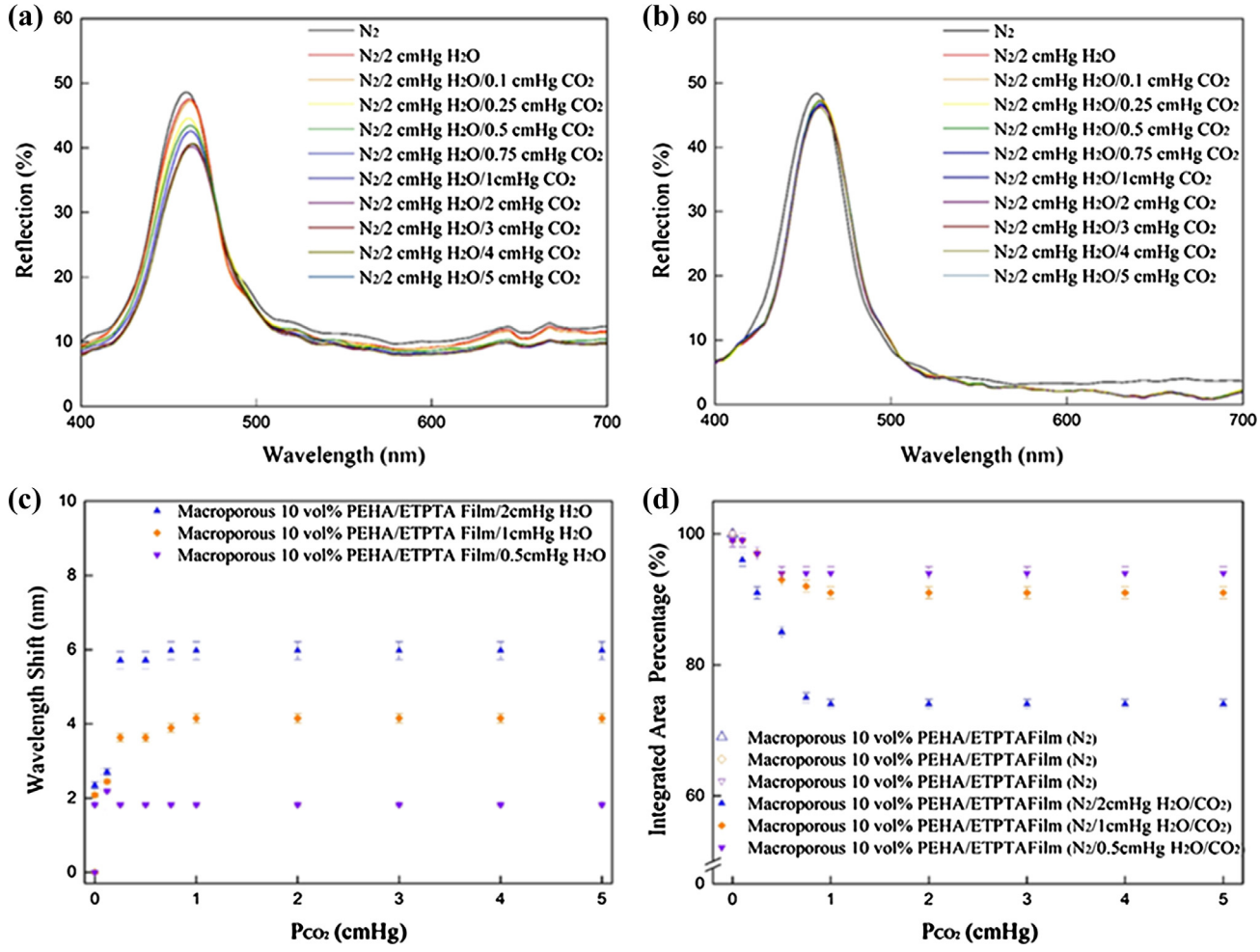

Fig. 8. Normal incidence optical reflection spectra obtained from macroporous 10 vol% PEHA/ETPTA films templated from 250 nm silica colloidal crystals exposed to carbon dioxide with different partial pressures in the presence of water vapor at (a) 1 cm Hg and (b) 0.5 cm Hg, respectively. (c) Dependence of the wavelength shift of the Bragg's diffraction peak on carbon dioxide partial pressure. (d) Dependence of the integrated response of the Bragg's diffraction peak on carbon dioxide partial pressure.

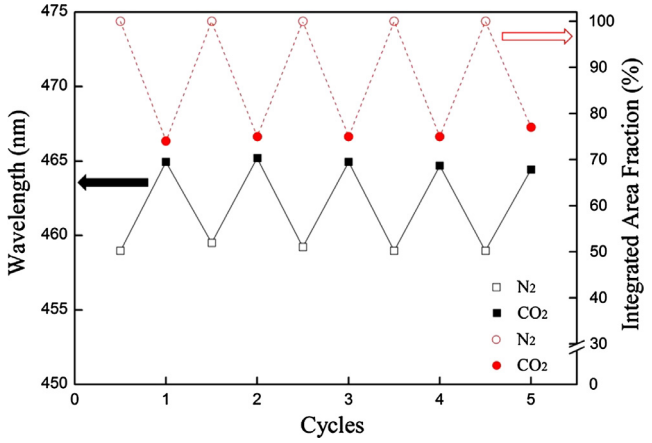

Fig. 9. Reversible carbon dioxide sensing of a macroporous 10 vol% PEHA/ETPTA film templated from 250 nm silica colloidal crystals.

to evaluate its durability. As presented in Fig. 9, the conversions of the diffraction peak position and amplitude upon adsorption and desorption of carbon dioxide and water are reversible and repeatable after 5 cycles. This indicates the use of macrporous ETPTA film as a scaffold provides a reversible and reproducible platform for sensing.

4. Conclusions

In summary, we develop a roll-to-roll compatible self-assembly technology to fabricate three-dimensional amine-functionalized photonic crystals. The photonic crystals display a visible readout for carbon dioxide response in several minutes through the combination of ordered macroporous structures and the strong adsorption of carbon dioxide to amine-functionalized surface. It is worth mentioning that the sensing performances can be improved by increasing the amount of amine groups coated on the macroporous photonic crystals, facilitating visual detection ranges from 0.1 cm Hg carbon dioxide partial pressure to 1 cm Hg carbon dioxide partial pressure in which post substantial human health hazards. To achieve lower detection limits, further work is underway to increase the surface area to volume ratio through introducing smaller silica particles. Importantly, the use of macrporous polymer scaffold results in a great reversibility for carbon dioxide sensing. Therefore, a rapid and visual sensor with reversibility and high selectivity for the sensing of carbon dioxide can be prepared. The methodology provides a simple and scalable route for preparing portable macroporous photonic crystals with various functional groups to expand the responsive ability, which is of great importance in on-line real-time monitoring and will find promising applications in the field of pH monitoring, chemical sensing, and biological sensing etc.

Acknowledgments

Acknowledgment is made to Ministry of Science and Technology (Grant MOST 105-2221-E-005-090) for support of this research.

Appendix A. Supplementary material

Supplementary data associated with this article can be found, in the online version, at http://dx.doi.org/10.1016/j.jcis.2017.07.031.

References

[1] C.L. Sabine, R.A. Feely, N. Gruber, R.M. Key, K. Lee, J.L. Bullister, R. Wanninkhof, C.S. Wong, B. Tilbrook, F.J. Millero, T.-H. Peng, A. Kozyr, T. Ono, A.F. Rios, Science 305 (2004) 62–69.
[2] M. Scheffer, V. Brovkin, P.M. Cox, Res. Lett. 2006, 33, 10702(1)-10702(4).
[3] X. Wang, H. Li, H. Liu, X. Hou, Micropor. Mesopor. Mat. 142 (2011) 564–569.
[4] M.M. Khader1, M.J. Al-Marri, S.Ali, G. Qi, E.P. Giannelis, Am. J. Analyt. Chem. 2015, 6, 274-284.
[5] P.A. Hernandez, K. Notsu, J.M. Salazar, T. Mori, G. Natale, H. Okada, G. Virgili, Y. Shimoike, M. Sato, N.M. Perez, Science 292 (2001) 83–86.
[6] R. Pierantozzi, Encyclopedia of chemical technology, fourth ed., Willey, New York, NY, 1991.
[7] T. Krishnakumar, R. Jayaprakash, T. Prakash, D. Sathyaraj, N. Donato, S. Licoccia, M. Latino, A. Stassi, G. Neri, Nanotechnology 2011, 22, 325501(1)-325501(8).
[8] J. Herran, G.G. Mandayo, E. Castano, Thin Solid Film 517 (2009) 6192–6197.
[9] A. Mills, S. Hodgern, Topics in fluorescence spectroscopy, Springer, Berlin, 2005.
[10] H.-K. Lee, N.-J. Choi, S.-E. Monn, J.-A. Heo, W.-S. Yang, J. Kim, J. Nanosci. Nanotechnol. 15 (2015) 404–407.
[11] J. Herran, O. Fernandez-Gonzalez, I. Castro-Hurtado, T. Romenro, G.G. Mandayo, E. Castano, Sens. Actuators B-Chem. 149 (2010) 368–372.
[12] Y.-F. Sun, S.-B. Liu, F.-L. Meng, J.-Y. Liu, Z. Jin, L.-T. Kong, J.-H. Liu, Sensors 12 (2012) 2610–2631.
[13] T.A. Vincent, J.-W. Gardner, Sens. Actuators B-Chem. 236 (2016) 954–964.
[14] J.R. Stetter, Chem. Rev. 108 (2008) 352–366.
[15] R.A. Potyrailo, C. Surman, N. Nagraj, A. Burns, Chem. Rev. 111 (2011) 7315–7354.
[16] A. Star, T.-R. Has, V. Joshi, J.-C.P. Gabriel, G. Gruner, Adv. Mater. 16 (2004) 2049–2052.
[17] J.D. Joannopoulos, R.D. Meade, J.N. Winn, Princeton University Press, Princeton, 1995.
[18] S. John, Phys. Rev. Lett. 58 (1987) 2486–2489.
[19] H. Härmä, S. Laakso, S. Pihlasalo, P. Hänninen, B. Faure, S. Rana, L. Bergström, Nanoscale 2 (2010) 69–71.
[20] L.L. Duan, B. You, L.M. Wu, M. Chen, J. Colloid Interface Sci. 353 (2011) 163–168.
[21] H. Kim, J. Ge, J. Kim, S. Choi, H. Lee, W. Park, Y. Yin, S. Kwon, Nature Photon. 3 (2009) 534–540.
[22] Y. Fang, Y. Ni, S.-Y. Leo, B. Wang, V. Basile, C. Taylor, P. Jiang, ACS Appl. Mater. Interfaces 7 (2015) 23650–23659.
[23] Y. Fang, Y. Ni, S.-Y. Leo, C. Taylor, V. Basile, P. Jiang, Nat. Commun. 6 (2015) 7416.
[24] T.S. Shim, S.H. Kim, J.Y. Sim, J.M. Lim, S.M. Yang, Adv. Mater. 22 (2010) 4494–4498.
[25] H. Yang, P. Jiang, B. Jiang, J. Colloid Interface Sci. 370 (2012) 11–18.
[26] B.H. King, A. Gramada, J.R. Link, M. Sailor, J. Adv. Mater. 19 (2007) 4044–4048.
[27] A.M. Ruminski, M.M. Moore, M.J. Sailor, Adv. Funct. Mater. 18 (2008) 3418–3426.
[28] P.J. Ge, Y.D. Yin, Angew. Chem. Int. Ed. 50 (2011) 1492–1522.
[29] L. Ripoll-Seguer, M. Beneito-Cambra, J.M. Herrero-Martínez, E.F. Simó-Alfonso, G. Ramis-Ramos, J. Chromatogr. A 1320 (2013) 66–71.
[30] D. Norton, S.A. Shamsi, Anal. Chem. 79 (2007) 9459–9470.
[31] C. Zhou, X. Gong, J. Han, R. Guo, Soft Mater. 11 (2015) 2555–2562.
[32] P. Jiang, M.J. McFarland, J. Am. Chem. Soc. 126 (2004) 13778–13786.
[33] L. Cui, Y. Yi, J. Wang, E. Tian, X. Zhang, Y. Zhang, Y. Song, L. Jiang, J. Mater. Chem. 19 (2009) 5499–5502.
[34] B. Prevo, O.D. Velev, Langmuir 20 (2004) 2099–2107.
[35] J. Wang, G.Y. Lee, R. Kennard, G. Barillaro, R.H. Bisiewicz, N.A.C. Lemus, X.C. Cao, E.J. Anglin, J.S. Park, A. Potocny, D. Bernhard, J. Li, M.J. Sailor, Chem. Mater. 29 (2017) 1263–1272.
[36] Q. Fu, B. Zhu, J. Ge, Nanoscale 9 (2017) 2457–2463.
[37] J.R. Oh, J.H. Moon, S. Yoon, C.R. Park, C.R. Do, J. Mater. Chem. 21 (2011) 14167–14172.
[38] E. Tian, J. Wang, Y. Zhang, Y. Song, L. Jiang, D. Zhu, J. Mater. Chem. 18 (2008) 1116–1122.
[39] O.S. Wolfbeis, J. Mater. Chem. 15 (2005) 2657–2669.
[40] W. Hong, Y. Chen, X. Feng, Y. Yan, X. Hu, B. Zhao, D. Zhang, Z. Xu, Y. Lai, Chem. Commun. 49 (2013) 8229–8231.
[41] M.G. Rabbani, H.M. El-Kaderi, Chem. Mater. 23 (2011) 1650–1653.
[42] W. Hong, Y. Chen, X. Feng, Y. Yan, X. Hu, B. Zhao, F. Zhang, D. Zhang, Z. Xu, Y. Lai, Chem. Commun. 49 (2013) 8229–8231.
[43] S.-H. Chai, Z.-M. Liu, K. Huang, S. Tan, S. Dai, Ind. Eng. Chem. Res. 55 (2016) 7355–7361.
[44] W. StÖber, A. Fink, E. Bohn, J. Colloid Interface Sci. 26 (1968) 62–69.
[45] G. Gonzalez, X. Fernandez-Francos, A. Serra, M. Sangermano, X. Ramis, Poly. Chem. 6 (2015) 6987–6997.
[46] C.-Y. Cai, K.-Y.A. Lin, Y.-C. Chen, H. Yang, Appl. Phys. Lett. 108 (2016) 071906.
[47] P. Jiang, J.F. Bertone, K.S. Hwang, V.L. Colvin, Chem. Mater. 11 (1999) 2132–2140.
[48] N.B. Colthup, L.H. Daly, S.E. Wiberly, Introduction to Infrared and Raman Spectroscopy, third ed., Academic Press, San Diego, CA, 1990.
[49] N. Hiyoshi, K. Yogo, T. Yashima, Microporous Mesoporous Mater. 84 (2005) 357–365.
[50] A. Danon, P.C. Stair, E. Weitz, J. Phys. Chem. C 115 (2011) 11540–11549.

[51] H. He, M. Zhong, D. Konkolewicz, K. Yacatto, T. Rappold, G. Sugar, N.E. David, J. Gelb, N. Kotwal, A. Merkle, K. Matyjaszewski, Adv. Funct. Mater. 23 (2013) 4720–4728.
[52] A. Goeppert, M. Czaun, R.B. May, G.K.S. Prakash, G.A. Olah, S.R. Narayanan, J. Am. Chem. Soc. 133 (2011) 20164–20167.
[53] B. Lv, B. Guo, Z. Zhou, G. Jing, Environ. Sci. Technol. 49 (2015) 10728–10735.
[54] M. Kampa, E. Castanas, Environ. Pollut. 151 (2008) 362–367.
[55] J. Zhang, J. Liu, Q. Peng, X. Wang, J. Li, Chem. Mater. 18 (2006) 867–871.
[56] H. Xu, P. Wu, C. Zhu, A. Elbaz, Z.Z.J. Gu, Mater. Chem. C 1 (2013) 6087–6098.
[57] A. Peeters, R. Ameloot, D.E. De Vos, Green Chem. 15 (2013) 1550–1557.